IEEE Photonics Journal
An IEEE Photonics Society Publication

Coherent Multimode OAM Superpositions for Multidimensional Modulation

Volume 6, Number 2, April 2014

Jaime A. Anguita, Member, IEEE
Joaquín Herreros
Ivan B. Djordjevic, Senior Member, IEEE

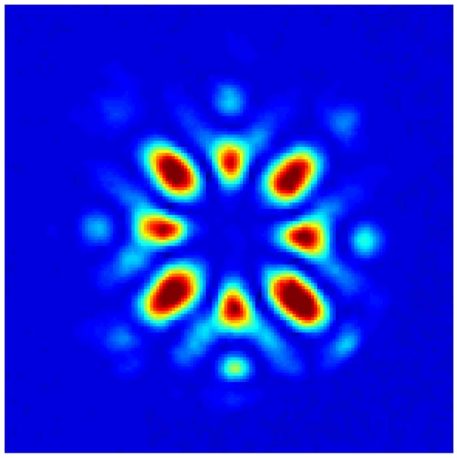

DOI: 10.1109/JPHOT.2014.2309645
1943-0655 © 2014 IEEE

Coherent Multimode OAM Superpositions for Multidimensional Modulation

Jaime A. Anguita,[1] ***Member, IEEE*****, Joaquín Herreros,**[1] **and Ivan B. Djordjevic,**[2] ***Senior Member, IEEE***

[1]Facultad de Ingeniería y Ciencias Aplicadas, Universidad de los Andes, Santiago 12445, Chile
[2]Department of Electrical and Computer Engineering, University of Arizona, Tucson, AZ 85721-0104 USA

DOI: 10.1109/JPHOT.2014.2309645

Manuscript received January 21, 2014; revised February 20, 2014; accepted February 23, 2014. Date of publication March 4, 2014; date of current version March 12, 2014. This work was supported in part by the Chilean Science and Technology Commission (CONICYT) under Grant Fondecyt 1120971 and in part by the NSF under Grant CCF-0952711. Corresponding author: J. A. Anguita (e-mail: janguita@miuandes.cl).

Abstract: The generation, propagation, and detection of high-quality and coherently superimposed optical vortices, carrying two or more orbital angular momentum (OAM) states, is experimentally demonstrated using an optical arrangement based on spatial light modulators. We compare our results with numerical simulations and show that, in the context of turbulence-free wireless optical communication (indoor or satellite), individual OAM state identification at the receiver of an OAM-modulated system can be achieved with good precision, to accommodate for high-dimensional OAM modulation architectures. We apply our results to the simulation of a communication system using low-density parity-check-coded modulation that considers optimal signal constellation design in a channel that includes OAM crosstalk induced by realistic (imperfect) detection.

Index Terms: Orbital angular momentum, optical vortices, free-space optical communications, optical modulation, satellite communications, data-center communications.

1. Introduction

Optical vortices are an interesting manifestation of phase singularities in laser beams and, consequently, have been studied with great interest from different outlooks. The ability to generate optical vortices has been demonstrated in several ways, and vortices can now be used for particle manipulation [1].

Increasing the information throughput and reliability of optical communication links—fiber-based and free-space—is one of the key aspects required to make this technology a suitable means to provide connectivity between high-speed networks or to deliver a bridge between wireless radio-frequency and long-haul optical networks, when other solutions are not attainable. By the same token, these aspects would also make free-space optical (FSO) links a competing solution for ground-to-satellite or inter-satellite communications. Increasing the photon efficiency by means of multidimensional modulation formats using all properties of optical beams is one way of achieving this goal. It has been proposed that beams carrying orbital angular momentum (OAM) can increase the information throughput in optical communications over unguided channels [2]. From the classical optics perspective, OAM is a property present in some optical beams that feature a helical wavefront. Such beams are usually denoted as vortices due to the phase discontinuity at their

optical axis [3]. The phase discontinuity produces a dark central spot in the intensity profile. A vector normal to a vortex wavefront follows a spiral trajectory around the optical propagation axis. The momentum of a vortex field is proportional to the number of turns that this vector completes around the beam's axis after propagating a distance equal to one wavelength. This number is equal to the OAM state.

OAM can be imposed to FSO beams. Some of the free-space modes that can transport OAM are Bessel beams, Hermite-Bessel beams, helical Mathieu beams, and Laguerre-Gauss beams [1], [3]–[7]. Laguerre-Gauss beams have been chosen, in many cases, for their simplicity of generation. Optical vortices with distinct integer topology (orbital momentum state) can be used to augment the data throughput and improve the bandwidth efficiency of indoor (e.g., data centers) and outdoor (e.g., terrestrial and satellite) optical wireless communication (OWC) links by allocating orthogonal channels that could simultaneously carry the information from different users, or to increment the dimensionality of a modulation constellation [8]–[11].

In this paper, we present an analytical derivation of the phase structure required to generate coherent OAM superpositions and simulate some particular cases (Section 2), we experimentally demonstrate the generation and detection of beams formed by coherent OAM state superpositions (Section 3), and we propose and evaluate a LDPC-precoded architecture using coherent OAM superpositions for an optimal signal constellation, N-dimensional modulation scheme, that includes the realistic effects of imperfect alignment and detection of the OAM-based system (Section 4). Concluding remarks are given in Section 5.

2. Generation and Detection of LG beams

2.1. Single-State LG Beams

The electric field of an LG beam can be expressed in cylindrical coordinates by [9]

$$u(r,\phi,z) = \sqrt{\frac{2p!}{\pi(p+|m|)!}}\frac{1}{w(z)}\left[\frac{r\sqrt{2}}{w(z)}\right]^{|m|} L_p^m\left[\frac{2r^2}{w^2(z)}\right] \times \exp\left[\frac{-r^2}{w^2(z)}\right]\exp\left[\frac{-ikr^2 z}{2\left(z^2+z_R^2\right)}\right] \times \exp\left[i(2p+|m|+1)\tan^{-1}\frac{z}{z_R}\right]\exp(-im\phi) \quad (1)$$

where $w(z) = w_0\sqrt{1+(z/z_R)^2}$ is the beam radius at distance z, w_0 is the radius of the zero-order Gaussian beam at the waist, $z_R = \pi w_0^2/\lambda$ is the Rayleigh range, λ is the optical wavelength, and $k = 2\pi/\lambda$ is the propagation constant. In (1), it is assumed that the beam waist is at $z = 0$. The term $L_p^m(\cdot)$ designates the generalized Laguerre polynomial, and p and m are the radial and angular mode numbers, respectively. The intensity profile of an LG beam is described by a set of $(p+1)$ concentric rings.

There are several ways to add OAM to a zero-order beam. Among them, we find spiral phase plates, wedges, diffraction gratings, and computer-controlled spatial light modulators (SLMs). Because of the mutual orthogonality between the electric fields of modes with different integer OAM states, one can—in principle—superimpose as many modes as one wishes and subsequently analyze (i.e., separate the components of) the multi-mode beam by optical means. The possibility of OAM state superpositions using diffractive elements provides the possibility of designing OAM-based modulation schemes, as part of an FSO communication link.

LG modes can be produced by a head-on incidence of a zero-order Gaussian beam onto the diffractive device programmed with a spiral phase distribution, like that of Fig. 1(a). This phase structure corresponds to the phase terms in (1) evaluated using $p = 0$, $m = 10$, and $z = 0$. In the head-on case, the diffractive orders will coincide on the optical axis, making the zero order

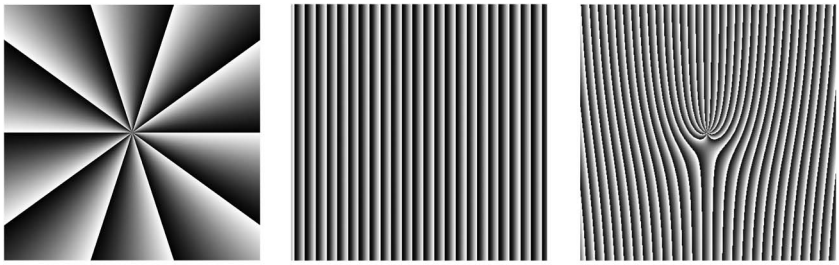

(a) (b) (c)

Fig. 1. (a) On-axis phase distribution of OAM state 10. (b) Zero-order blazed grating. (c) Interference phase pattern between (a) and (b).

propagate along with the LG mode. This is undesirable in some design cases, and an angled incidence may be preferred. In the angled case, the phase structure must then be constructed by creating an interference pattern between the aforementioned spiral phase pattern and the phase pattern of an angled plane wave [e.g., Fig. 1(b)]. The resulting phase pattern would, in this case, be that of Fig. 1(c). The incident beam must be aimed to the phase dislocation to produce good-quality LG beams. The resulting grating will produce several orders (depending on the grating type) along a plane perpendicular to the grating lines. In our experiments, the unwanted orders are purposely blocked after a few tens of centimeters.

2.2. Beams With Mutually-Coherent OAM Superpositions

It has been shown that it is possible to spatially split the vortices of a high-order mode—initially on a single optical axis—into a collection of vortices with separated cores [12]. The generation of two mutually-coherent vortices with a common axis has been accomplished using dove prisms in double paths [13]. Also, the so-called optical ferris wheels resulting from the superpositions of two coherent vortices with certain state combinations have been demonstrated to trap atoms [14].

Generating multiple-state LG beams can also be achieved by designing an artificial multi-vortex interference pattern and recording it onto a computer-generated hologram or by programming an SLM. The diffraction induced by this pattern will generate a superposition of OAM states whose electric fields are mutually-coherent if a single optical source is shone onto the diffracting device. The superimposed states will propagate together and may be distinguished and separated using a second diffractive device programmed with one or more of the constituent modes.

Given that these diffractive operations are performed using small diameter beams (e.g., 2 or 3 mm in diameter) and the grating's pitch is a fraction of a millimeter, the diffraction orders are fanned out at relatively short distances ($<$ 1 m).

2.3. Generation of Superimposed Vortices Using an SLM

In the experimental work presented here, we have used reflective SLMs as generating and analyzing devices to demonstrate the feasibility of the principle and, thus, of the proposed modulation. The gratings are created by adding the electric fields of all the constituent states, each of which is given by (1), and afterwards extracting only the phase elements of the superposition. Note that adding only the phase terms of the constituent states will not produce the desired phase pattern, as the contributing phases would not be properly balanced.

We chose to use a radial parameter $p = 0$, so that each individual mode is a single ring. At the beam waists (i.e., $z = 0$), the electric field is reduced to

$$u^m(r,\phi) = \underbrace{\sqrt{\frac{2}{\pi}}\frac{1}{w_0}\exp\left[-\frac{r^2}{w_0^2}\right]}_{A(r)} \underbrace{\sqrt{\frac{1}{|m|!}}\left(\frac{r\sqrt{2}}{w_0}\right)^{|m|}}_{R(r,m)} \exp(-im\phi) \tag{2}$$

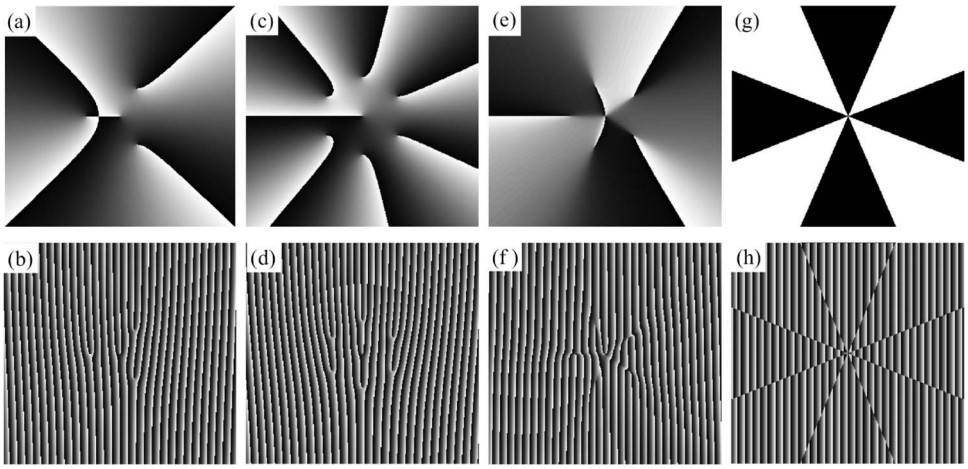

Fig. 2. On-axis and off-axis phase structures of two-mode superpositions based on (8): (a)–(b) $(m_1, m_2) = (1, 4)$; (c)–(d) $(m_1, m_2) = (1, 7)$; (e)–(f) $(m_1, m_2) = (2, -3)$; (g)–(h) $(m_1, m_2) = (4, -4)$.

so that it can be written as

$$u^m(r,\phi) = A(r)R(r,m)\exp(-im\phi).$$

For two LG modes with the same waist diameter w_0 and states m_1 and m_2, respectively, the superposition is simply

$$u^{m_1,m_2}(r,\phi) = u^{m_1}(r,\phi) + u^{m_2}(r,\phi) \tag{3}$$

$$= A(r)[R(r,m_1)\exp(-im_1\phi) + R(r,m_2)\exp(-im_2\phi)]. \tag{4}$$

In order to find the total phase, we reorganize the components to isolate the real terms

$$\frac{u^{m_1,m_2}(r,\phi)}{A(r)R(r,m_1)} = \exp(-im_1\phi) + \frac{R(r,m_2)}{R(r,m_1)}\exp(-im_2\phi) \tag{5}$$

where

$$\zeta(r,m_2,m_1) \triangleq \frac{R(r,m_2)}{R(r,m_1)} = \sqrt{\frac{|m_1|!}{|m_2|!}}\left(\frac{r\sqrt{2}}{w_0}\right)^{|m_2|-|m_1|} \tag{6}$$

is a scalar that weighs the combination of constituent phase terms (analogous to the radius shown in [15] and [16]). By expanding the complex exponentials, one obtains

$$\frac{u^{m_1,m_2}(r,\phi)}{A(r)R(r,m_1)} = \cos(m_1\phi) + \zeta(r,m_2,m_1)\cos(m_2\phi) - i[\sin(m_1\phi) + \zeta(r,m_2,m_1)\sin(m_2\phi)]. \tag{7}$$

Therefore, given that $A(r)R(m_1) \in \mathbb{R}$, the phase term of the LG superposition $u^{m_1,m_2}(r,\phi)$ (rotated in π rads to drop the – sign) is the angle

$$\Theta_{w_0}^{m_1,m_2}(r,\phi) = \arctan\left[\frac{\sin(m_1\phi) + \sqrt{\frac{|m_1|!}{|m_2|!}}\left(\frac{r\sqrt{2}}{w_0}\right)^{|m_2|-|m_1|}\sin(m_2\phi)}{\cos(m_1\phi) + \sqrt{\frac{|m_1|!}{|m_2|!}}\left(\frac{r\sqrt{2}}{w_0}\right)^{|m_2|-|m_1|}\cos(m_2\phi)}\right]. \tag{8}$$

This spatial phase distribution is used to simulate the superpositions shown in Fig. 2, whose first and second rows depict the on-axis phase and the off-axis phase, respectively. The latter is

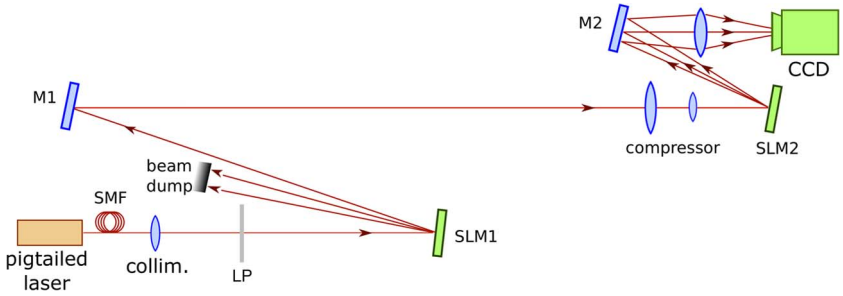

Fig. 3. Simplified schematic of the optical setup of the multi-mode OAM experiment.

obtained by modulating (8) with an angle of incidence θ as

$$P_{(m_1,m_2)}(x,y) = \left[kx\sin\theta - \Theta_{w_0}^{m_1,m_2}(r,\phi)\right] \pmod{2\pi}. \tag{9}$$

The examples in Fig. 2(a)–(h) correspond to the superpositions $(m_1, m_2) = (1, 4)$, $(m_1, m_2) = (1, 7)$, $(m_1, m_2) = (2, -3)$, and $(m_1, m_2) = (4, -4)$, respectively. Note that arctan in (8) is a four-quadrant function. This simple procedure can be numerically extended to find the superposition of three or more OAM states, from which one can obtain the desired phase structure to be programmed on a grating.

2.4. Detection Using an SLM

The orthogonality between the component modes in a coherent superposition allows their subsequent separation using optical means. A mode can be singled out using a complex conjugate version of its electric field [9]. OAM analyzers may use a phase pattern identical to that of the LG mode subject to detection, but with opposite OAM state sign. This transformation—also programmed onto an SLM on the receiver side—cancels the OAM, and the beam can focus on a zero-order spot at the far field (achieved using a converging lens) [17]. This spot can be sensed with a communication detector to recover the transmitted information.

A detection grating can have more than one spatial dimension to allow simultaneous detections [2]. An efficient detection scheme requires diffraction patterns that distinguish several modes simultaneously. Each analyzed mode diffracts to a different angle and can be focused with one or more lenses. In this proof of concept, we demonstrate the quality of the superimposed LG modes by detecting single constituent states at a time, using one-dimensional gratings like that of Fig. 1(c). This helps make the features more apparent to the reader.

3. Experimental Demonstration

3.1. Description of Optical Setup

Our proof of concept is evaluated with the following setup. A single-mode pigtailed red laser (660 nm) is collimated with an aspheric lens. The emerging beam has a mode field diameter of approximately 3 mm and is filtered with a linear polarizer to match the polarization of the transmit SLM. To achieve the small-incidence angles ($<$ 1 deg) required to match the pitch of the grating, the path is folded using small mirrors. The transmit SLM is programmed with a series of phase patters, according (8) and (9), and produces a few diffraction orders, although a large fraction of the power remains on orders $\{-1, 0, +1\}$. After a few tens of centimeters, the unwanted orders are blocked. The superposition of LG modes (on order $+1$) is propagated over about 7 m on a folded path, after which is compressed using a Galilean telescope and aligned to the analyzing SLM. This SLM is programmed with a sinusoidal fork grating (instead of a blazed grating) to balance the power on diffraction orders $\{-1, +1\}$. The diffracted pattern is focused on a CCD camera. A simplified diagram is given in Fig. 3.

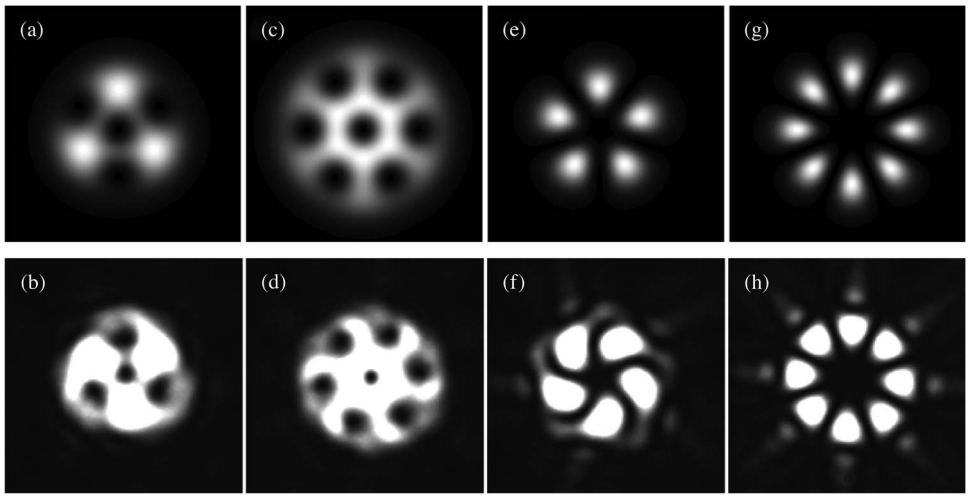

Fig. 4. Simulated (first row) and experimental (second row) intensity patterns of the coherent two-mode superpositions whose grating patterns are shown in Fig. 2. (a)–(b) $(m_1, m_2) = (1, 4)$; (c)–(d) $(m_1, m_2) = (1, 7)$; (e)–(f) $(m_1, m_2) = (2, -3)$; (g)–(h) $(m_1, m_2) = (4, -4)$.

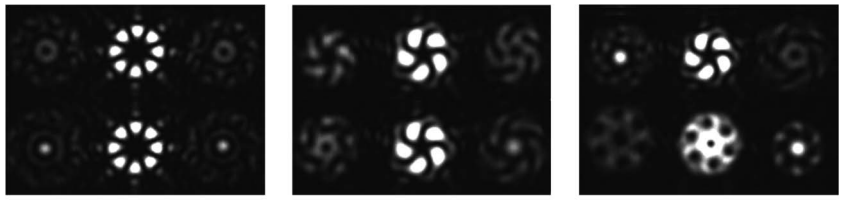

Fig. 5. Experimental detection of individual OAM states from a received coherent two-state superposition. (a) Combination (4, −4) detected using OAM state 3 (top) and state 4 (bottom). (b) Combination (2, −3) detected using OAM state 1 (top) and state 2 (bottom). (c) Combination (2, −3) detected using OAM state 3 (top, −3 is focused) and combination (1, 7) detected using state 1 (bottom).

3.2. Combination of Two Modes

In Fig. 4, we show the intensity profiles based both on computer simulations (constructed by electric-field addition at $z = 0$) and experimental measurement (as seen by the camera after the analyzing SLM on diffraction order 0). These coherent superpositions of OAM states correspond to the phase patterns shown in Fig. 2. The agreement between the simulations and experimental results is very good in all cases, and the slight differences are due to beam rotation and some image saturation.

3.3. Detection of Constituent States

To demonstrate the effectiveness of individual OAM state detection at the receiver, we present six examples corresponding to the OAM modes previously discussed. Detection occurs at the center of the diffraction orders +1 and −1 produced by the receive SLM. In Fig. 5, each horizontal line-up corresponds to diffraction orders +1, 0, and −1. In (a), received superposition (4, −4) is detected using state 3 (top image) and using state 4 (bottom image, where both states are detected simultaneously). In (b), received superposition (2, −3) is detected using state 1 (top image) and using state 2 (bottom image). In (c), the same combination is detected using state 3 (top image), but the energy then focuses on order +1, corresponding to the detection of state −3. Combination (1, 7) [(c), bottom image] is detected using state 1. Very little energy crosstalk will be induced between modes if adequate apertures (pin holes) are used for signal separation. We found that, by

(a) (b) (c)

Fig. 6. Coherent superposition of four OAM states. (a) Numerical simulation and (b) experimental realization for the coherent superposition of $\{\pm 4, \pm 8\}$. (c) Experimental superposition of states $\{\pm 2, \pm 6\}$.

simulating the use of 50-μm pin holes over the images of the detected modes, average crosstalk values of -10 dB are found for adjacent states [e.g., a detection like that of Fig. 5(a) top] and an average of -25 dB for two-state differences.

3.4. Combination of Four Modes

Three-mode or larger superpositions can be designed by numerically extending the method proposed above. We present two examples of four-state coherent superpositions: $(-8, -4, 4, 8)$ and $(-6, -2, 2, 6)$, that have balanced state numbers and produce $x - y$ symmetric patterns. The simulated and experimental intensity pattern for combination $(-8, -4, 4, 8)$ is shown in Fig. 6(a) and (b), respectively. The difference between the two is due to beam rotation and a small mismatch in the beam diameter illuminating the SLM. Fig. 6(c) shows the pattern for $(-6, -2, 2, 6)$.

4. OSCD-Based OAM Modulation

In our previous publication [11], the multidimensional constellation for communication over FSO channel affected by atmospheric turbulence has been obtained as an N-dimensional Cartesian product of pulse amplitude modulation (PAM). Direct detection was used in that case. It has been recently shown [18] that multidimensional signal constellations obtained by optimum signal constellation design (OSCD) algorithm [19], [20] can significantly outperform conventional modulations and even sphere-packing based constellations, when multidimensional coded modulation has been used in few-mode fiber (FMF)-based applications.

In this work, we employ a similar strategy but study the OAM-based multidimensional coded modulation for use in turbulence-free OWCs. The key idea is to dramatically increase the data rate delivered to the end user in turbulence-free optical wireless links. This approach is suitable for use in data-center applications, indoor OWCs, and inter-satellite communications.

In what follows, we use the OAM modes generated in Section 3 as the basis functions for multidimensional signaling by taking the imperfect generation of OAM modes into account. The multidimensional signaling is based on OSCD algorithm developed in [19], which results in channel capacity achieving signal constellations. This approach is motivated by the need to improve the energy efficiency of OWCs.

4.1. Description of OSCD-Based OAM LDPC-Coded Modulation

The overall system architecture is shown in Fig. 7. A continuous wave (CW) laser diode signal is split into N branches by using a power splitter (such as 1: N star coupler) to feed N electro-optical modulators—such as Mach–Zehnder modulators (MZMz)—each corresponding to one out of the N OAM states. The jth input to the jth MZM, $1 \leq j \leq N$ corresponds to the jth coordinate of the signal constellation point to be transmitted. The N TEM_{00} modes, upon modulation, are shone on a series of diffracting devices (volume holograms or SLMs could be used for this purpose), each programmed to one out of the N OAM states being used. The corresponding diffraction angles are

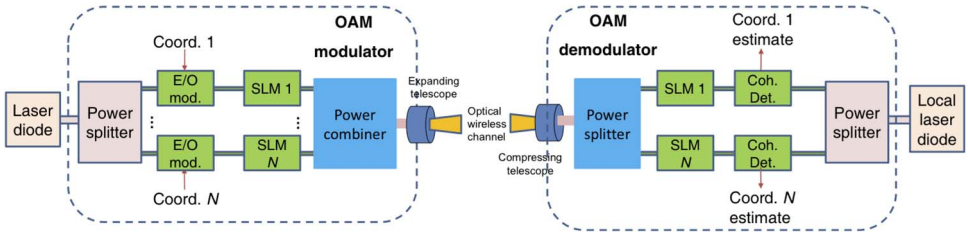

Fig. 7. General FSO system configuration utilizing OAM-based N-dimensional modulation. Optical signal is transmitted through a single aperture.

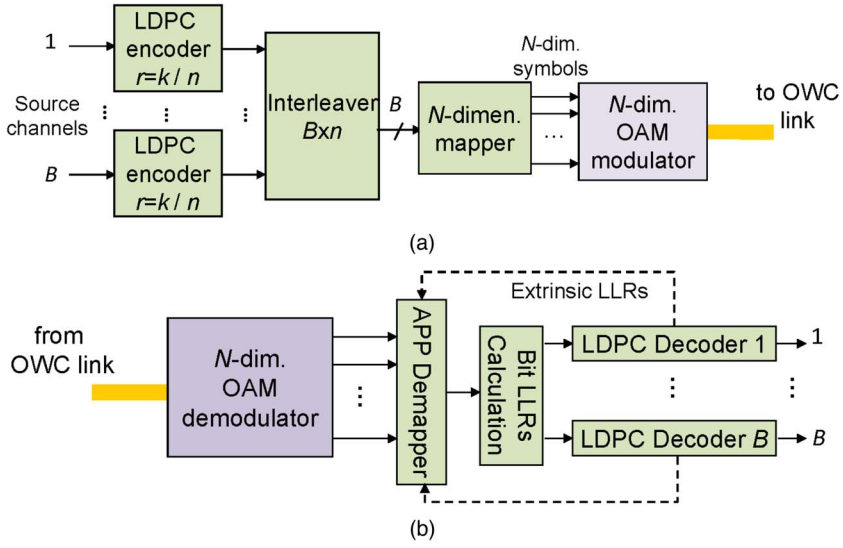

Fig. 8. Operational diagram of the communication system utilizing coherent superposition of OAM states and LDPC coded optimal signal constellation design (OSCD). (a) Transmitter configuration. (b) Receiver configuration.

adjusted so that coaxial propagation of outgoing OAM beams is obtained, and the resulting superposition beam is directed toward the receiver side by an expanding telescope.

The signal constellation points of *M*-ary OSCD are generated as described in [18]. The coordinates of the OSCD signal constellation are used as the inputs to the *N*-dimensional OAM modulator, as shown in Fig. 8(a). This modulator generates the signal constellation points as

$$s_i = C \sum_{j=1}^{N} \phi_{i,j} \Phi_i \tag{10}$$

where $\phi_{i,j}$ denotes the *j*th OAM coordinate ($j = 1, \ldots, N$) of the *i*th signal-constellation point, and the set $\{\Phi_1, \ldots, \Phi_N\}$ represents the set of *N* orthogonal OAM eigenstates. As an illustration in Fig. 9, we show 8-ary 3D-OSCD constellation: (a) in the presence of noise (at SNR of 30 dB) and (b) in the presence of noise and imperfect generation of OAM states, causing the crosstalk among coordinates.

On the receiver side, we first perform the *N*-dimensional OAM demodulation, as shown in Fig. 7. The demodulator outputs, after sampling, the projections on each OAM basis function *j*, $\forall j \in (j = 1, \ldots, N)$. For coherent detection, one local laser diode is used for detection of all OAM coordinates. To keep the receiver complexity reasonably low, only in-phase components should be used. By using this approach, only 3-dB couplers are needed to mix the incoming OAM projections and the local laser signal followed by corresponding photodetectors.

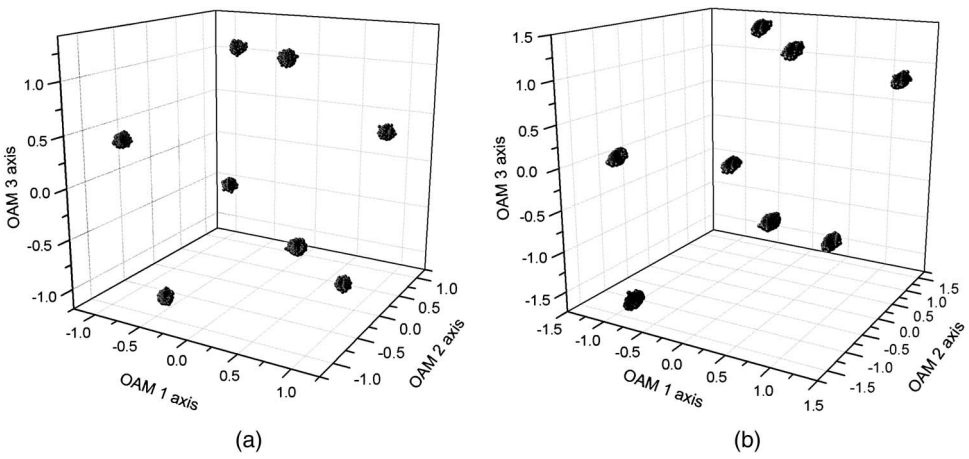

Fig. 9. Constellation of OAM modulation points. In (a) the signal elements are only affected by additive noise. In (b), OAM signal crosstalk induced by imperfect alignment and detection is included.

A block diagram of the transmitter architecture is shown in Fig. 8(a). The B binary data streams are encoded using B (n, k) LDPC codes of reasonably large codeword lengths. The codewords generated by LDPC encoders are written row-wise into the corresponding block-interleaver. The B bits at time instance i are taken column-wise from the block-interleaver and are used as the input to the corresponding N-dimensional mapper, implemented as a look-up table (LUT). The N coordinates from the N-dimensional mapper are used as inputs to the N-dimensional modulator, which generates the signal constellation points according to (10).

The block diagram for the receiver architecture is shown in Fig. 8(b). The reconstructed OAM coordinates, taken from the N-dimensional demodulator outputs, are used as inputs to an N-dimensional a posteriori probability (APP) demapper, which calculates symbol log-likelihood ratios (LLRs). From symbol LLRs, we determine bit LLRs, in a so-called bit-LLRs calculator [see Fig. 8(b)], and pass them to the corresponding LDPC decoders. After LDPC decoding, the extrinsic information is passed back to the APP demapper. We iterate the extrinsic information between LDPC decoders and APP demapper until convergence or a pre-determined number of iterations has been reached. This procedure is similar to that described in [21].

4.2. BER Performance Analysis

In order to illustrate the high potential of the proposed OSCD-based LDPC-coded OAM modulation, we perform the Monte Carlo simulations by using the OAM basis functions obtained experimentally. We include the effects of OAM crosstalk, whose values are described in Section 3.3. The results of simulations for (girth-10, column-weight-3, regular, quasi-cyclic) LDPC (16935, 13550)-coded OAM modulation are summarized in Fig. 10(a). On the other hand, the results of simulations for (girth-8, column-weight-4, regular, quasi-cyclic) LDPC (4320, 3242)-coded N-dimensional OAM modulations are presented in Fig. 10(b). The aggregate data rate can be calculated by $\log_2(M)R_s r$, where M is the signal constellation size, R_s is the symbol rate, and r is the code rate (0.8 in the example from Fig. 10). For example, by setting $R_s = 25$ GS/s and $M = 16$, the aggregate data rate of 100 Gb/s is obtained, which is compatible with 100G Ethernet. (The 16-QAM constellation is defined over two OAM states.) The improvement of $N = 2$, $M = 16$ OSCD-based LDPC coded OAM modulation over conventional LDPC-coded 16-QAM, for the following crosstalk distribution from neighboring OAM coordinates (-10 dB and -25 dB), is even 1.57 dB at BER $= 10^{-8}$. On the other hand, the improvement of 3-D 16-ary constellation over 16-QAM is a fantastic 3.44 dB at the same BER. As we increase the number of dimensions, BER performances are less sensitive to imperfect generation or alignment of OAM modes. For instance, for the same BER and crosstalk distribution, the degradation for 16-QAM is 0.81 dB, while degradation for 8-ary 3D-OSCD is 0.31 dB. However, the degradation for 8-ary 4D-OSCD is only 0.25 dB at BER $= 10^{-8}$.

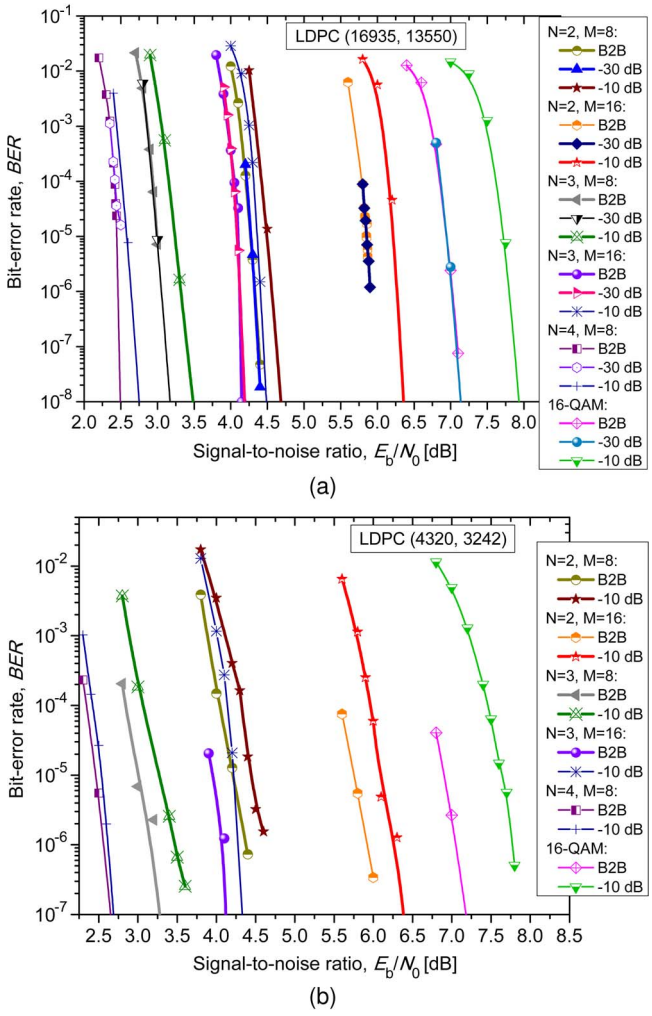

Fig. 10. Bit-error rate using codes (16935, 13550), rate 0.8 and (4320, 3242), rate 0.75.

5. Concluding Remarks

We demonstrate that coherent multi-mode OAM beams can be generated and detected for use in an OAM-modulated communication link. Experimental results show that high-quality multi-mode generation is possible, as compared with numerical simulation. We provide an analytical basis for two-state OAM superpositions and experimentally demonstrate that individual mode detection (separation) is possible and with good precision. OAM superpositions with up to four states are demonstrated. We propose the use of OAM state superpositions for high-dimensional modulation while including the effects of imperfect detection that may appear with the use of SLMs or other diffractive devices.

The exponential Internet traffic growth projections have placed enormous transmission rate demand on the underlying information infrastructure at every level, from the core to access networks. The 100 Gb/s Ethernet (100 GbE) standard has been adopted recently (IEEE 802.3ba), and 400 GbE and 1 Tb/s Ethernet (1 TbE) are being considered by many authors as the next natural steps. Higher volumes of traffic have also increased the energy consumption of transmission and switching equipment needed to route this traffic. Therefore, the Internet has become constrained not only by capacity but also by its energy consumption. In order to solve capacity and energy-efficiency problems of future Internet technologies simultaneously, we proposed the use of OSCD-based

N-dimensional LDPC-coded OAM modulation for OWCs. This scheme can be used to achieve beyond 100 Gb/s transmission, for reasonable small signal constellation sizes, while employing the state-of-the-art 25-Gb/s technology. The proposed scheme represents a promising candidate for various applications, including indoor OWC data center applications and satellite links.

References

[1] C. López-Mariscal, J. C. Gutiérrez-Vega, G. Milne, and K. Dholakia, "Orbital angular momentum transfer in helical Mathieu beams," *Opt. Exp.*, vol. 14, no. 9, pp. 4182–4187, May 2006.

[2] G. Gibson, J. Courtial, and M. J. Padgett, "Free-space information transfer using light beams carrying orbital angular momentum," *Opt. Exp.*, vol. 12, no. 22, pp. 5448–5456, Nov. 2004.

[3] L. Allen, M. W. Beijersbergen, R. J. C. Spreeuw, and J. P. Woerdman, "Orbital angular momentum of light and the transformation of Laguerre-Gaussian laser modes," *Phys. Rev. A*, vol. 45, no. 11, pp. 8185–8189, Jun. 1992.

[4] Z. Bouchal, J. Wagner, and M. Chlup, "Self-reconstruction of a distorted nondiffracting beam," *Opt. Commun.*, vol. 151, no. 4–6, pp. 207–211, Jun. 1998.

[5] W. C. Soares, D. P. Caetano, and J. M. Hickmann, "Hermite-Bessel beams and the geometrical representation of nondiffracting beams with orbital angular momentum," *Opt. Exp.*, vol. 14, no. 11, pp. 4577–4582, May 2006.

[6] D. Rozas, C. T. Law, and G. A. Swartzlander, Jr., "Propagation dynamics of optical vortices," *J. Opt. Soc. Amer. B, Opt. Phys.*, vol. 14, no. 11, pp. 3054–3065, Nov. 1997.

[7] A. Vaziri, G. Weihs, and A. Zeilinger, "Superpositions of the orbital angular momentum for applications in quantum experiments," *J. Opt. B, Quantum Semiclass. Opt.*, vol. 4, no. 2, pp. S47–S51, Apr. 2002.

[8] J. Lin, X.-C. Yuan, S. H. Tao, and R. E. Burge, "Multiplexing free-space optical signals using superimposed collinear orbital angular momentum states," *Appl. Opt.*, vol. 46, no. 21, pp. 4680–4685, Jul. 2007.

[9] J. A. Anguita, M. A. Neifeld, and B. Vasic, "Turbulence-induced channel crosstalk in an orbital angular momentum-multiplexed free-space optical link," *Appl Opt.*, vol. 47, no. 13, pp. 2414–2429, May 2008.

[10] J. Wang, J.-Y. Yang, I. M. Fazal, N. Ahmed, Y. Yan, H. Huang, Y. Ren, Y. Yue, S. Dolinar, M. Tur, and A. E. Willner, "Terabit free-space data transmission employing orbital angular momentum multiplexing," *Nat. Photon.*, vol. 6, no. 7, pp. 488–496, Jul. 2012.

[11] I. B. Djordjevic, J. Anguita, and B. Vasic, "Error-correction coded orbital-angular-momentum modulation for FSO channels affected by turbulence," *J. Lightwave Technol.*, vol. 30, no. 17, pp. 2846–2852, Sep. 2012.

[12] A. Kumar, P. Vaity, and R. P. Singh, "Crafting the core asymmetry to lift the degeneracy of optical vortices," *Opt. Exp.*, vol. 19, no. 7, pp. 6182–6190, Mar. 2011.

[13] Y.-D. Liu, C. Gaoa, M. Gaoa, X. Qi, and H. Weber, "Superposition and detection of two helical beams for optical orbital angular momentum communication," *Opt. Commun.*, vol. 281, no. 14, pp. 3636–3639, Jul. 2008.

[14] S. Franke-Arnold, J. Leach, M. J. Padgett, V. E. Lembessis, D. Ellinas, A. J. Wright, J. M. Girkin, P. Ohberg, and A. S. Arnold, "Optical ferris wheel for ultracold atoms," *Opt. Exp.*, vol. 15, no. 14, pp. 8619–8625, Jul. 2007.

[15] E. J. Galvez, N. Smiley, and N. Fernandes, "Composite optical vortices formed by collinear Laguerre-Gauss beams," in *Proc. SPIE*, 2006, vol. 6131, pp. 19–26.

[16] S. M. Baumann, D. M. Kalb, L. H. MacMillan, and E. J. Galvez, "Propagation dynamics of optical vortices due to Gouy phase," *Opt. Exp.*, vol. 17, no. 12, pp. 9818–9827, Jun. 2009.

[17] J. A. Anguita and C. Quezada, "Demonstration of orbital-angular-momentum-based multiple-channel free-space communication," presented at the Latin America Optics Photonics Conference, Sao Sebastiao, Brazil, 2012, Paper LM4C.5.

[18] I. B. Djordjevic, T. Liu, L. Xu, and T. Wang, "On the multidimensional signal constellation design for few-mode fiber based high-speed optical transmission," *IEEE Photon. J.*, vol. 4, no. 5, pp. 1325–1332, Oct. 2012.

[19] T. Liu and I. B. Djordjevic, "On the optimum signal constellation design for high-speed optical transport networks," *Opt. Exp.*, vol. 20, no. 18, pp. 20 396–20 406, Aug. 2012.

[20] I. B. Djordjevic, "On the irregular nonbinary QC-LDPC-coded hybrid multidimensional OSCD-modulation enabling beyond 100 Tb/s optical transport," *J. Lightwave Technol.*, vol. 31, no. 16, pp. 2969–2975, Aug. 2013.

[21] I. B. Djordjevic, "Spatial-domain-based hybrid multidimensional coded-modulation schemes enabling multi-Tb/s optical transport," *J. Lightwave Technol.*, vol. 30, no. 14, pp. 2315–2328, Jul. 2012.